Immunometabolism and immunomodulation in the airways

Novel strategies to treat pneumonia

Ramirez Moral, I.

Publication date
2022

CHAPTER 2

mTOR-driven glycolysis governs induction of innate immune responses by bronchial epithelial cells exposed to the bacterial component flagellin

I. Ramirez-Moral, X. Yu, J. M. Butler, M. van Weeghel, N. A. Otto, B. Lima Ferreira, L. Van Maele, J. C. Sirard, A. F. de Vos, M. D. de Jong, R. H. Houtkooper and T. van der Poll

Mucosal Immunol. 2021 May;14(3):594-604

ABSTRACT

Human bronchial epithelial (HBE) cells play an essential role during bacterial infections of the airways by sensing pathogens and orchestrating protective immune responses. We here sought to determine which metabolic pathways are utilized by HBE cells to mount innate immune responses upon exposure to a relevant bacterial agonist. Stimulation of HBE cells by the bacterial component flagellin triggered activation of the mTOR pathway resulting in an increased glycolytic flux that sustained the secretory activity of immune mediators by HBE cells. The mTOR inhibitor rapamycin impeded glycolysis and limited flagellin-induced secretion of immune mediators. The role of the mTOR pathway was recapitulated *in vivo* in a mouse model of flagellin-triggered lung innate immune responses. These data demonstrate that metabolic reprogramming via the mTOR pathway modulates activation of the respiratory epithelium, identifying mTOR as a potential therapeutic target to modulate mucosal immunity in the context of bacterial infections.

INTRODUCTION

The airways are constantly exposed to potentially harmful agents including microbes and airway epithelial cells represent the first line of defense[1]. Besides playing a role in maintaining the air-tissue barrier, airway epithelial cells have the ability to recognize bacterial components and secrete a wide range of mediators required to initiate and orchestrate a protective immune response against potentially harmful bacteria[2]. Depending on the stimulus respiratory epithelial cells can secrete inflammatory mediators in a polarized manner, either to the basal or luminal side[3]. In recent years much insight has been generated into the role of immunometabolism in host defense against pathogens; especially metabolic reprogramming of leukocytes upon interaction with bacterial components has received significant attention[4,5]. Cells use distinct metabolic pathways to generate energy and biosynthetic intermediates to exert their function[6]. Proinflammatory responses typically are associated with a shift toward glycolysis, while anti-inflammatory responses are usually associated with enhanced activity of the tricarboxylic acid (TCA) cycle and oxidative phosphorylation[6]. Mammalian target of rapamycin (mTOR) has been implicated as a central regulator of intracellular metabolism in several immune cell types, and amongst other, stimulates glycolysis[7]. However, studies investigating airway epithelial cell function are scarce and dominated by investigations using epithelial cell lines, in which metabolism is intrinsically altered[8], or *in vivo* mouse models[9,10]. At present, it is unknown whether metabolic reprogramming mediates functional innate immune responses in primary human bronchial epithelial (HBE) cells upon activation by bacterial agonists. Here, we cultured primary HBE cells in an air–liquid interface mimicking the human airways[11,12] to address this question. HBE cells highly express Toll-like receptor 5 (TLR5) that recognizes the bacterial component flagellin, one of the main constituents of flagella present in pneumonia-causing pathogens such as *Pseudomonas aeruginosa*[13]. Upon sensing, TLR5 activation results in the production of various pro-inflammatory cytokines and chemokines by epithelial cells[14]. Administration of flagellin via the airways has been suggested as an immune enhancing adjunctive therapy in pneumonia[14]. Here, we sought to determine the metabolic adaptations in HBE cells upon activation by flagellin and their role in immune activation. We show

that the mTOR pathway is a crucial regulatory node between the metabolic and immune status of HBE cells upon flagellin exposure, suggesting that modulation of the mTOR pathway might be an interesting therapeutic approach in airway inflammatory diseases caused by bacteria.

RESULTS

Human bronchial epithelial cells respond selectively to different bacterial stimuli

We first determined the ability of different Gram-negative bacteria to activate HBE cells. For this, we exposed HBE cells to the common human respiratory pathogens *Klebsiella pneumoniae* and *Pseudomonas aeruginosa* (UV-inactivated) and measured the release of the chemokines CXCL1, CXCL8, CCL20, and granulocyte colony-stimulating factor (G-CSF) as surrogate markers of HBE innate immune responses. Stimulation with whole inactivated pathogens strongly triggered polarized release of CXCL8, CCL20, and CXCL1 to the basolateral side (**Figures 1a** and **S1a**) and G-CSF to the apical side (**Figures 1b** and **S1b**). This was accompanied by an induction of the corresponding genes as well as upregulation of *DEFB4A*, the gene encoding the antimicrobial peptide β-defensin2 (**Figure 1c**). Next, we sought to determine if either lipopolysaccharide (LPS) or flagellin alone, two components present in many Gram-negative bacteria, were able to activate HBE cells. The TLR4 ligand LPS was unable to induce the release of the prototypic HBE cell chemokines (**Figures 1a, b**), which is in line with previous observations.15 The TLR5 ligand flagellin induced the polarized release of CXCL8, CCL20, and CXCL1 to the basolateral side (**Figure 1a**) and G-CSF to the apical side (**Figure 1b**) as well as enhanced expression of the corresponding genes (**Figure 1c**).

Besides TLR5, flagellin can activate the inflammasome component NLR family CARD domain-containing protein 4 (NLRC4)[14]. Cytokines that rely on inflammasomes for release of their mature forms include IL-1β and IL-18. NLRC4 can mediate the generation of mature IL-1β and IL-18 from their respective pro-forms through activation of caspase-1. While flagellin induced *IL1B* gene expression, IL-1β secretion did not occur to a significant extent; *IL18* was not induced by flagellin (**Figure S2**). These data are consistent with previous studies that documented the potency of flagellin to activate respiratory epithelial cells[14,16,17] and suggest an important role of TLR5 signaling in HBE cell activation.

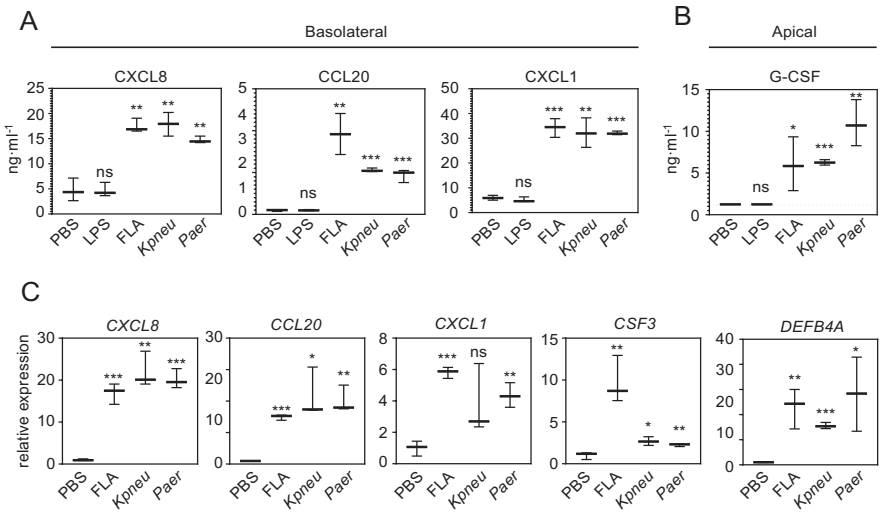

Figure 1 Human bronchial epithelial cells respond selectively to microbial stimuli. CXCL8, CCL20, and CXCL1 levels in the basolateral compartment (**a**) and G-CSF levels in the apical wash (**b**) of untreated HBE cells (PBS) or stimulated for 24 h with LPS (100 ng/ml), flagellin (FLA, 1 µg/ml), UV-inactivated *Klebsiella pneumoniae* (*Kpneu*) or *Pseudomonas aeruginosa* (*Paer*) (1:2 cell:bacteria). (**c**) Fold increase of mRNA expression for the indicated immune mediators (normalized to the housekeeping gene HPRT) in HBE cells from **a** relative to the unstimulated control (PBS). Data in **a–c** are presented as box and whisker plots (n = 3–4 per group). *p* values were calculated using Student's *t* test compared to unstimulated cells. $*p < 0.05$; $**p < 0.01$; $***p < 0.001$, ns not significant.

Flagellin shifts the metabolic profile of HBE cells toward carbohydrates

Next, we investigated changes in cellular metabolism in HBE cells after flagellin activation aiming to find new targets to modulate the innate immune function of HBE cells. For this we assessed genome-wide gene expression by RNA sequencing in HBE cells stimulated with flagellin (or PBS control) for 24 h. Flagellin elicited profound changes in the HBE cell transcriptome with 1916 genes differentially expressed when compared to PBS control (**Figure 2a**). Pathway analysis showed that flagellin as expected induced overexpression of genes encoding factors related to signaling pathways implicated in innate immunity;

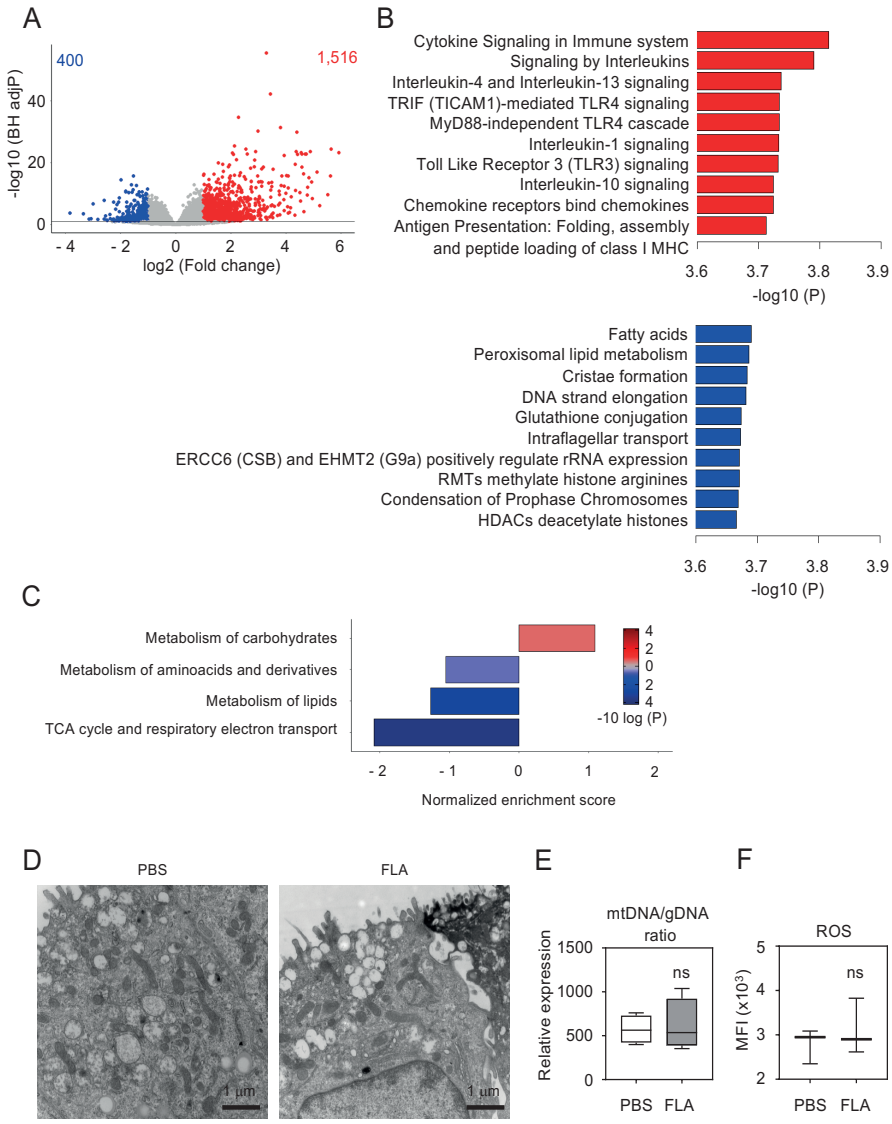

Figure 2 Flagellin shifts the metabolic profile of HBE cells toward carbohydrates. (**a**) Volcano plot representation (integrating multiple-test adjusted *p* values and log2-fold changes) of genome-wide transcriptome differences in HBE cells after incubation with flagellin or PBS (control) for 24 h. In red up-regulated genes; in blue downregulated genes. Horizontal line represents the multiple-test adjusted significance threshold (Benjamini–Hochberg adjusted $p < 0.05$). (**b**) Pathway analysis from **a** showing pathways enriched for

Figure 2 (continuation) up-regulated (red) or downregulated genes (blue). (**c**) Pathway analysis of transcriptional response in energy metabolism pathways in HBE cells upon flagellin stimulation for 24 h relative to unstimulated control cells. In red pathways enriched with up-regulated genes; in blue pathways enriched with downregulated genes. Adjusted *p* values were calculated using Benjamini–Hochberg adjustment. (**d**) Mitochondrial morphology assessed by electron microscopy. (**e**) Mitochondrial mass as measured by mitochondrial (mt)-DNA/genomic (g)-DNA ratio. *p* value was calculated using Student's *t* test compared to unstimulated cells. ns not significant. (**f**) Reactive oxygen species (ROS) levels as measured with carboxy-H2DCFDA. *p* value was calculated using Student's *t* test compared to PBS control. ns not significant. Data in **a–c** comprises three biological donors in duplicate from two independent experiments (n = 6). Data in **e** and **f** are displayed as box and whisker plots (n = 3–4 per group).

remarkably, flagellin treatment downregulated pathways included fatty acids and lipid metabolism-related pathways (**Figure 2b**). Transcriptomic analysis of flagellin-induced genes involved in the main energy metabolism pathways revealed that the only metabolic pathway enriched with over-expressed genes was carbohydrate metabolism, while other energy metabolism pathways (aminoacids, lipids, and the TCA cycle and respiratory electron transport chain) were downregulated (**Figure 2c**). Mitochondrial morphology has been suggested as an indicator of mitochondrial function.18 Using electron microscopy, we found no changes in mitochondrial morphology that can be attributed to flagellin stimulation (**Figure 2d**). To further assess mitochondrial function, we examined the abundance of mitochondria and found no differences in mitochondrial mass attributed to flagellin stimulation (**Figure 2e**). In addition, flagellin did not induce the generation of reactive oxygen species (ROS) compared to control (**Figure 2f**). Supporting these findings, we found no differences in gene set enrichment analysis (GSEA)[19] in the ROS generation pathway from RNAseq data (**Figure S3**). These data show that flagellin produces robust alterations in the energy metabolism of HBE cells and suggest that flagellin induces a metabolic shift toward enhanced carbohydrate metabolism.

Glycolysis controls flagellin-induced activation of HBE cells

Considering the observed upregulation of genes involved in glucose metabolism we sought to investigate the functional role of glucose metabolism in HBE cell activation upon flagellin challenge. We first analyzed glucose uptake in HBE cells. After 24 h of flagellin stimulation, HBE cells showed increased glucose uptake compared to unstimulated control cells (**Figure 3a**). To investigate whether the increased demand of glucose responded to a higher glycolytic metabolism, we assessed secretion of lactate, a hallmark of glycolysis. Indeed, 6 and 24 h after flagellin challenge, HBE cells secreted significantly more lactate than unstimulated control cells (**Figure 3b**). The rapid induction of glycolysis upon flagellin stimulation prompted us to investigate how stable isotope-labeled $^{13}C_6$-glucose is metabolized in HBE cells immediately following activation. In line with increased lactate accumulation, glucose-derived isotopologue of lactate (M + 3) was significantly increased 30 min after activation by flagellin (**Figure 3c**). At this early time point the TCA intermediates malate (M + 2) and α-ketoglutarate (M + 2) were also increased in flagellin-stimulated cells, while pyruvate (M + 3) and fumarate (M + 2) were not affected (**Figure S4A**). In total, 24 h after addition of flagellin, the intracellular levels of lactate were increased relative to medium control conditions, while the intracellular concentrations of pyruvate, fumarate, α-ketoglutarate, and malate were not altered (**Figure S4B**). These results suggest that HBE cells display a rapid and sustained glycolytic response following flagellin activation.

Additionally, supporting this observation, GSEA further confirmed the metabolic reliance on glycolysis in flagellin-stimulated HBE cells (**Figures. 3d** and **S5**). To investigate the functional role of glycolysis in the flagellin response of HBE cells more directly, we next assessed the effect of glycolysis inhibition on glucose metabolism and cell activation after flagellin stimulation. As expected, glucose uptake after flagellin stimulation was reduced by the glycolysis inhibitor 2-deoxyglucose (2-DG) (**Figure 3e**). The reduction in glucose uptake was accompanied by an impaired lactate production upon flagellin stimulation (**Figure 3f**). This 2-DG induced inhibition of glycolysis limited the ability of HBE cells to secrete CCL20 and CXCL1 to the basolateral compartment (**Figure 3g**) and G-CSF to the apical side (**Figure 3h**). Taken together, these data demonstrate that glycolysis is triggered by flagellin and that this metabolic pathway is functionally required for flagellin-induced chemokine production by HBE cells.

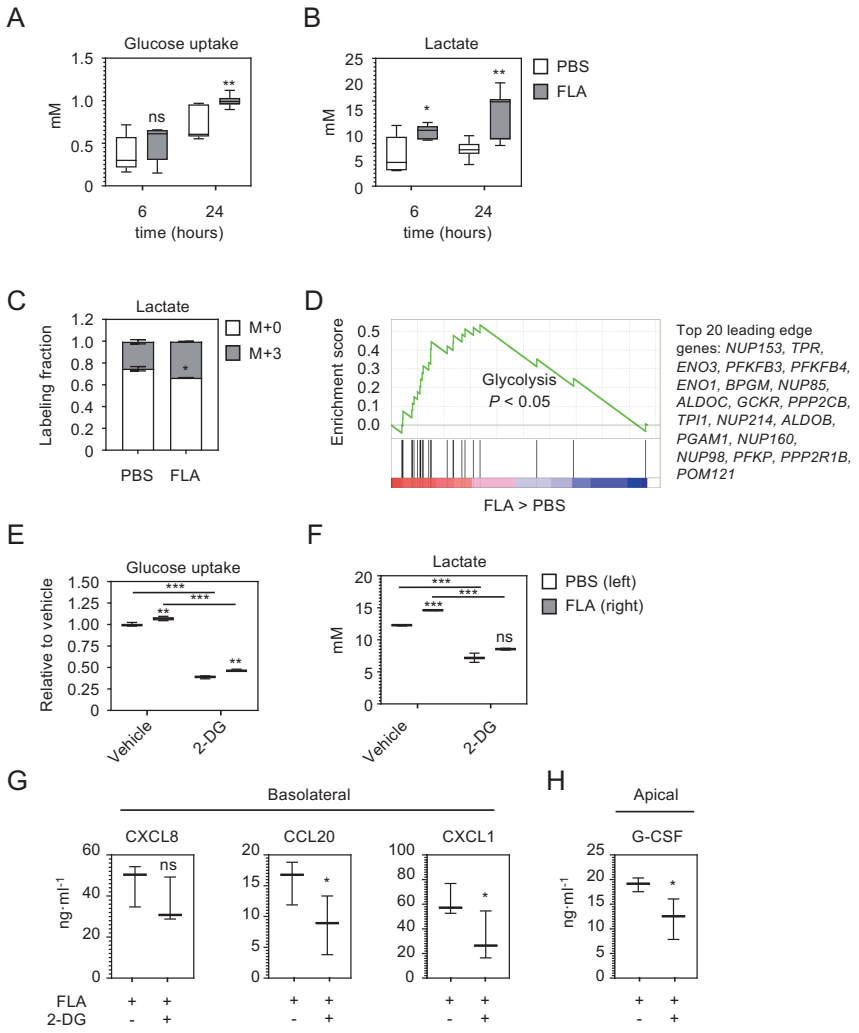

Figure 3 Glycolysis regulates flagellin-induced immune activation of HBE cells. Analysis of glucose uptake (**a**) and levels of lactate secreted to the culture medium (**b**) by HBE cells incubated with flagellin or PBS (control) for 6 or 24 h. c Glucose-derived carbon labeling of lactate in HBE cells 30 min after incubation with flagellin or PBS (control) in ^{13}C-glucose-containing media. Bar graphs show mass isotopologue distribution of incorporated label. M + 0 bars represent the fraction of lactate with no 13C-glucose incorporation. (**d**) Gene

Figure 3 (continuation) set enrichment analysis (GSEA) of the glycolysis pathway in HBE cells activated with flagellin for 24 h compared to unstimulated control cells (PBS). The x-

axis shows individual genes and the y-axis shows enrichment score. The 20 most enriched genes are listed. Red represents up-regulated genes and blue represents downregulated genes. Analysis of glucose uptake (**e**) and levels of lactate secreted to the culture medium (**f**) by HBE cells pretreated for 1 h with the glycolysis inhibitor 2-DG (5 mM) or vehicle and stimulated for 24 h with PBS or flagellin. CXCL8, CCL20, and CXCL1 levels in culture supernatant (**g**) and G-CSF in apical wash (**h**) of HBE cells incubated with flagellin or PBS (control) in the presence of 5 mM 2-DG of vehicle. Data in **a**, **b**, **e–h** are presented as box and whisker plots. **a**, **b**, n = 5–7 per group from three donors in duplicate; **c**, n = 3 replicates; **e**, **f**, n = 3–6 replicates per group representative of two independent experiments; **g**, **h**, n = 3 biological donors representative of two independent experiments. *p* values were calculated using Student's *t* test. **p* < 0.05; ***p* < 0.01; ****p* < 0.001, ns not significant. Data in **d** comprises three biological donors in duplicate from two independent experiments (n = 6).

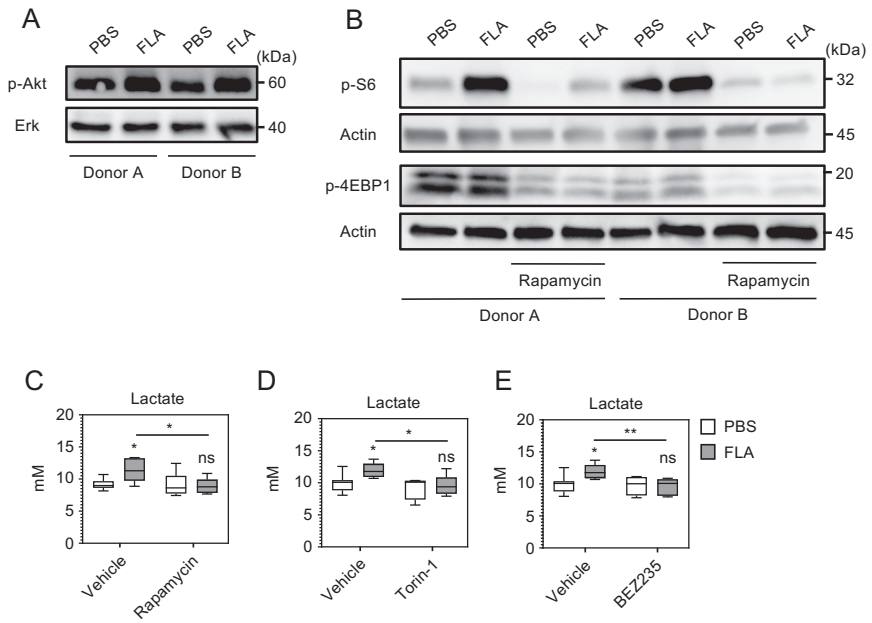

Figure 4 Akt-mTOR axis is triggered by flagellin and controls the glycolytic function of HBE cells. (**a**) Immunoblot analysis of phosphorylated (p-) Akt and total Erk (loading control), in

Figure 4 Akt (continuation) HBE cells from two donors, incubated with 1 µg/ml flagellin or PBS (control) for 2 h. (**b**) Immunoblot analysis of p-S6 and p-4EBP1, as well as total actin

(loading control), in HBE cells from two donors (**a, b**) incubated with flagellin or PBS (control) for 2 h with or without preincubation (1 h) with 10 nM rapamycin. Levels of lactate secreted to the culture medium by HBE cells pretreated for 1 h with the mTOR inhibitors rapamycin (10 nM) (**c**), torin-1 (100 nM) (**d**), BEZ235 (100 nM) (**e**), or vehicle and stimulated for 24 h with PBS or flagellin. For **c–e**, data are presented as box and whisker plots (n = 4–7 replicates per group including two individual donors). *p* values were calculated using Student's *t* test. **p* < 0.05; ***p* < 0.01; ****p* < 0.001; ns not significant.

Akt-mTOR axis is triggered by flagellin and controls the glycolytic function of HBE cells

The Akt-mTOR pathway is a master regulator of different cell functions, including glucose metabolism[20,21]. Here, we aimed to determine whether the higher glycolytic rate in HBE cells induced by flagellin is under the control of the mTOR pathway. Flagellin triggered the Akt-mTOR pathway, as indicated by increased phosphorylation of Akt (**Figure 4a**). Furthermore, the S6K1 substrate S6 ribosomal protein (S235/236) and 4E-BP1, two canonical downstream targets of mTOR,21 were activated upon flagellin stimulation (**Figure 4b**). Treatment with rapamycin inhibited flagellin-mediated induction of the mTOR pathway, as shown by diminished levels of phosphorylated S6 and 4E-BP1 (**Figure 4b**). Moreover, rapamycin treatment resulted in a significant reduction of lactate release after flagellin stimulation, indicating the involvement of the mTOR pathway in induction of glycolysis by flagellin (**Figure 4c**). Likewise, two other mTOR inhibitors (torin-1, a mTORC1-2 inhibitor21; and BEZ235, a PI3K-mTOR dual inhibitor22) inhibited flagellin-induced lactate secretion, confirming the involvement of the mTOR pathway in the regulation of glycolysis in HBE cells and ruling out an off-target effect of rapamycin (**Figures 4d, e**).

mTOR regulates HBE cell-immune function in response to flagellin

Our findings that glycolysis is necessary for chemokine release by HBE cells and that this metabolic pathway is under the control of mTOR prompted us to study the role of the mTOR pathway during immune activation of HBE cells through RNA sequencing analysis. This revealed profound rapamycin induced changes in the transcriptome of HBE cells activated by flagellin (**Figures S6A, B**). Of

interest, GSEA showed that rapamycin downregulated glycolysis (**Figure 5a**), further supporting the involvement of the mTOR pathway in the regulation of this energy pathway. A direct comparison of flagellin stimulation in the presence or absence of rapamycin showed that the mTOR pathway is crucial for the immune function of HBE cells. Most importantly, rapamycin suppressed the expression of genes encoding for immune mediators such as chemokines and antimicrobial peptides (**Figure 5b**; validation of selected mRNA's by RT-PCR in **Figure S7**). In line with these results, inhibition of the mTOR pathway limited the immune response of HBE cells typified by decreased CXCL8, CCL20, and CXCL1 to the basolateral side (**Figure 5c**) as well as reduced secretion of G-CSF to the apical compartment (**Figure 5d**). Together these data demonstrate that flagellin triggers mTOR-dependent glycolysis in HBE cells to induce an immune response.

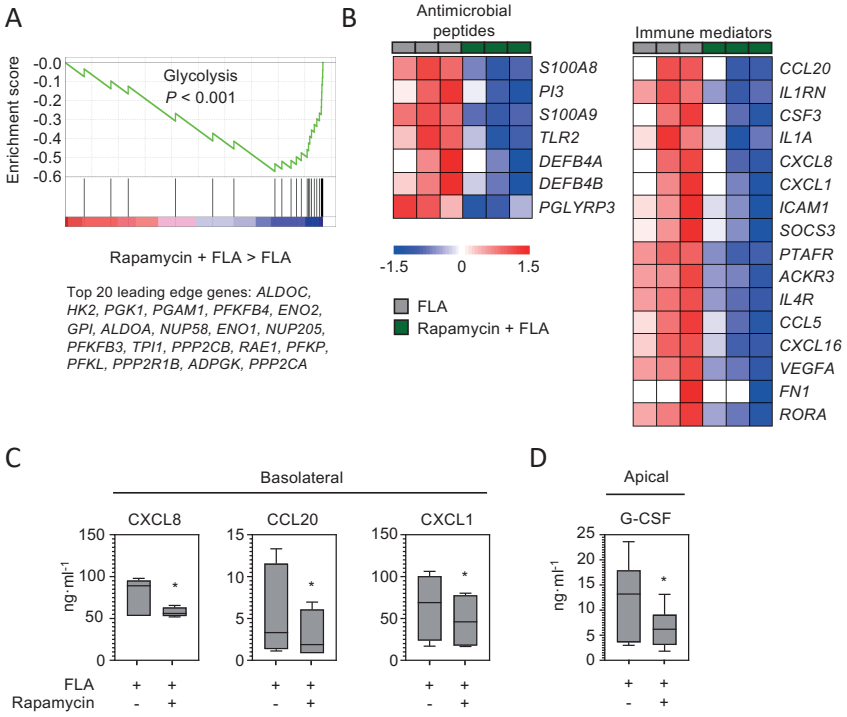

Figure 5 mTOR regulates HBE cell-immune function in response to flagellin. (**a**) Gene set enrichment analysis (GSEA) of the glycolysis pathway in HBE cells activated with flagellin **Figure 5** (continuation) for 24 h in the presence of either vehicle or 10 nM rapamycin (pretreated for 1 h). Log2-fold expression values were ranked in descending order. The x-

axis shows individual genes and the y-axis shows enrichment score. The 20 most enriched genes are listed. Red represents up-regulated genes and blue represents downregulated genes. (**b**) Heat-map of changes in the expression of selected flagellin-induced genes in HBE cells after 24 h in the presence of 10 nM rapamycin relative to vehicle. Red denotes high expression, blue indicates low expression. (**c**), (**d**) Secretion of CXCL8, CCL20, and CXCL1 to the basolateral compartment (c) and G-CSF to the apical side (**d**) by HBE cells in the presence of 10 nM rapamycin or vehicle added 1 h prior to addition of flagellin and stimulated for 24 h. Data in **a, b** comprise three biological donors in duplicate from two independent experiments (n = 6). Data in **c, d** are presented as box and whisker plots (n = 6 from three biological donors in duplicate). *p* values were calculated using Student's paired *t* test. $*p < 0.05$.

mTOR controls flagellin-induced inflammation in vivo

To study the consequences of mTOR inhibition during lung innate immune responses *in vivo*, we administered rapamycin or vehicle intraperitoneally both 24 and 1 h before challenging mice with flagellin via the airways. Flagellin triggered the glycolysis pathway in bronchial epithelial cells as reflected by a twofold increase in the expression of Hk2, the first enzyme of glycolysis, in bronchial brushes; this flagellin effect was prevented by treatment with rapamycin, indicating that mTOR also controls glycolysis in bronchial epithelial cells *in vivo* (**Figure 6a**). Flagellin induced the upregulation of epithelial cell-specific immune mediators such as *Cxcl1*, *Cxcl2*, and *Csf3* in bronchial brushes, responses that were almost abrogated by rapamycin (**Figure 6b**). This rapamycin effect was accompanied by inhibited flagellin-induced CXCL1 and CXCL2 release into bronchoalveolar lavage (BAL) fluid (**Figure 6c**). G-CSF remained undetectable in BAL fluid after flagellin administration.

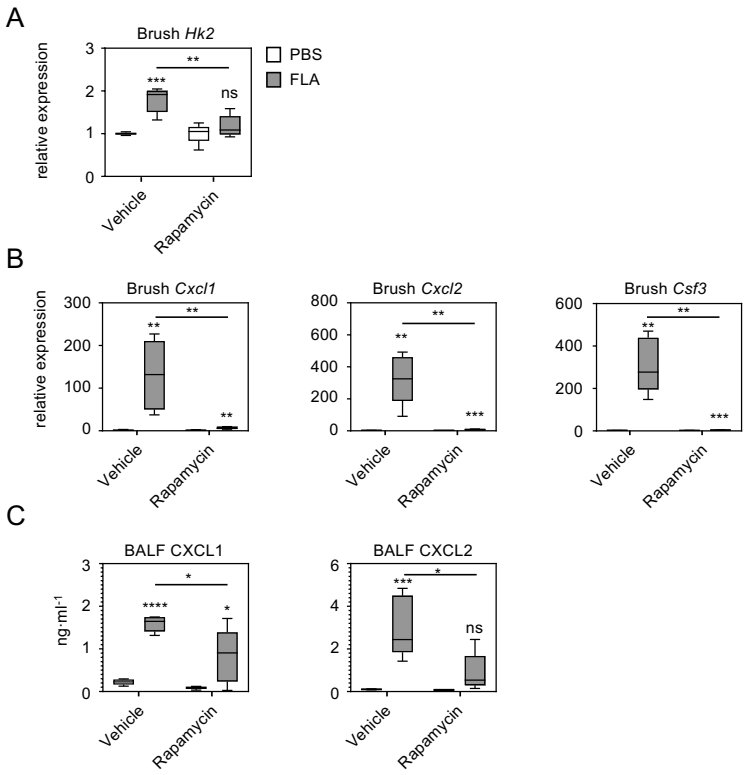

Figure 6 mTOR inhibition impairs lung epithelial cell responses to flagellin *in vivo*. (**a**), (**b**) Mice received rapamycin or vehicle 24 and 1 h prior to intranasal administration of flagellin or PBS and bronchial brushings were harvested 2 h after challenge for RNA extraction and qPCR analysis of the indicated genes. (**c**) CXCL1 and CXCL2 were measured in BAL fluid 2 h after the challenge with flagellin. Data are shown as box and whisker plots (n = 6 per group). *p* values were calculated using Student's *t* test. **p* < 0.05; ***p* < 0.01; ****p* < 0.001; *****p* < 0.0001. ns not significant.

DISCUSSION

Immune cells can rewire their metabolic program to rapidly fulfill their energy requirements in order to sustain an effective immune response. Together with immune cells, the airway epithelium represents the first line of defense against inhaled pathogens. While knowledge on metabolic control of innate immune responses by different leukocyte subsets has rapidly expanded in recent years[4,5], data on the role of cellular metabolism in airway epithelium responses remains scarce. Here we used primary HBE cells to demonstrate that the common mucosal pathogen component flagellin triggers aerobic glycolysis that is required to sustain the production of inflammatory mediators. Specifically, we show that this metabolic adaptation is in part under the control of the Akt-mTOR pathway. Inhibition of the mTOR pathway prevented the induction of glycolysis and limited the secretory capacity of the HBE cells in response to flagellin. These results were recapitulated in a mouse model of airway inflammation induced by flagellin *in vivo*. To the best of our knowledge our study is the first to report on energy metabolism pathways and mTOR function in primary human respiratory epithelial cells. The current results should be considered in the context of earlier studies on cellular metabolism in lymphocytes and myeloid cells[4,5,23,24]. T-cell receptor mediated activation results in mTOR activation, and while naive and tolerant T cells primarily use oxidative phosphorylation to produce ATP, activation toward T-effector cells requires extensive metabolic rewiring and a shift toward glycolysis[23,24]. Myeloid cells also experience metabolic reprogramming upon recognition of pathogens, which supports their activation and the initiation of an innate immune response. Whereas LPS elicits a similar metabolic shift toward glycolysis as observed in activated lymphocytes, other TLR ligands and intact pathogens may induce more complex alterations in energy metabolism pathways in monocytes[18]. In myeloid cells mTOR is a master regulator of metabolism, which can be activated by a variety of stimuli relevant in the context of infection, including TLR ligands and cytokines[7]. Intriguingly, activation of mTOR can have contrasting roles in distinct cells or models. The seemingly contrasting roles of mTOR in individual cells or models might have several explanations, including differences in experimental conditions, such as the analysis of primary cells versus cell lines, and differences between mice and humans concerning the importance of the arginine and nitric oxide system, which is regulated by mTOR[7].

In addition, the mTOR pathway is characterized by a high degree of complexity. As an example, inhibition of mTORC1 activates the PI3K-AKT pathway; distinct AKT isoforms stimulate different macrophage polarization states and the phosphorylation status of AKT changes substrate specificity[25]. Moreover, in different *in vivo* settings the relative importance of the mTOR pathway for an immune response versus other host mediators impacting this response determines the "inflammatory" contribution of mTOR to that response[7]. In myeloid cells inhibition of mTOR stimulates IL-12 expression while reducing IL-10 expression, suggesting an anti-inflammatory role for mTOR[26]. In contrast, tumor necrosis factor (TNF) and IL-6 production by myeloid cells are mostly blocked by rapamycin, indicating a pro-inflammatory role for mTOR[7]. Similarly, mTOR positively contributes to the expression of pro-inflammatory CXCL8, IL-6, and TNF in neutrophils[27]. We here report that mTOR clearly has a pro-inflammatory immune enhancing role in HBE cells stimulated with flagellin, as indicated by reduced expression of a large set of antimicrobial peptides and immune mediators in cells treated with rapamycin. In support of a pro-inflammatory role of mTOR in epithelial cells, a previous study using a respiratory epithelial cell line responsive to LPS reported reduced LPS-induced IL-6 and CXCL8 production after knockdown of mTOR by siRNA[28]. In this latter study[28] LPS was able to activate epithelial cells, contrasting with our data, which might be due to differences in the cells used (an HBE cell-line grown in submerged culture medium versus differentiated primary human HBE cells grown in air/liquid interface). One earlier study investigated the effects of flagellin on cellular metabolism: flagellin elicited mTOR activation in a mouse macrophage cell line and inhibition of mTOR by rapamycin diminished flagellin-induced TNF and IL-6 release by these cells[29]. We did not find evidence for an effect of flagellin on mitochondrial function in primary HBE cells. In a previous study flagellin was reported to induce mitochondrial dysfunction and increased ROS production in IB3-1 cells, an immortalized cell line created from bronchial epithelial cells isolated from a patient with cystic fibrosis[30]. Thus, flagellin effects on mitochondrial function in respiratory epithelial cells may differ between different experimental conditions. The effects of rapamycin in HBE cells were partially reproduced in mouse respiratory epithelial cells *in vivo*, as reflected by strongly reduced *Cxcl1, Cxcl2*, and *Csf3* expression in epithelial brushes and attenuated

CXCL1 and CXCL2 protein release in BAL fluid from mice administered with flagellin via the airways. These results are in agreement with an earlier study showing that selective disruption of *Mtor* in the respiratory epithelium of mice was associated with reduced release of CXCL1 and CXCL2 in BAL fluid upon intratracheal injection of LPS[28]; it would be of great interest to study the effects of flagellin in these genetically modified mice. Furthermore, rapamycin exerted protective anti-inflammatory effects in mouse models of LPS-induced acute lung injury[28,31]. Our investigation only studied the metabolic consequences of stimulation of HBE cells with flagellin, which has relevance for respiratory pathogens expressing this TLR5 ligand (most notably *P. aeruginosa*) as well as in the context of studies evaluating flagellin as a potential immune stimulating adjuvant in the treatment of airway infection[14]. We here showed that besides UV-inactivated *P. aeruginosa* also *K. pneumoniae* (an un-flagellated bacterium) activates primary HBE cells. Further research is needed to assess whether intact pathogens induce similar or more complex changes in energy metabolism pathways, such as has been documented in monocytes exposed to whole bacteria[18]. Our data do not proof that flagellin effects are mediated by TLR5. A role for the alternative flagellin receptor NLRC4 seems less likely considering the absence of IL-1β protein release in the presence of clear *IL1B* gene induction. Notably, primary human airway epithelial cells express high levels of TLR5 at their surface[32,33] and in mice flagellin promoted epithelial cell responses in a TLR5- dependent manner that did not require NLRC4 signaling[16]. mTOR consists of two complexes: mTORC1 and mTORC2[7]. Of these mTORC1 has been implicated in the regulation of metabolism and immune functions, while mTORC2 regulates cytoskeletal dynamics and activates AKT, which in turn can activate mTORC1. Rapamycin is a selective mTORC1 inhibitor and thus our findings are in agreement with a central role for mTORC1 in cellular metabolism and immunity[7]. The respiratory epithelium represents a first line of defense in the lungs and plays an essential role in mounting an innate immune response to pathogens that invade the lower airways. We here establish the mTOR-glycolysis axis as a key metabolic regulator of the host immune function in the airway epithelium in response to flagellin. These results increase current knowledge on mechanisms underlying activation of the respiratory epithelium during airway

inflammation and infection and may guide selection of therapeutic targets in these conditions.

ACKNOWLEDGEMENTS

I.R.-M. was funded by the Era-Net JPIAMR/ZonMW (grant 50-52900-98-201); X.Y. was funded by European Union's Seventh Framework project PREPARE (grant 602525); N.A.O. was funded by ZonMW (grant 40-00812-98-14016); B.L.F. was supported by FAPESP (grant 2019/02224-0), and J.-C.S. was funded by JPIAMR/ANR (ANR-15-JAMR0001-01). Part of this work was funded by European Union H2020 (FAIR project, grant 847786). The authors thank Linda Koster (Core Facility Genomics, Amsterdam UMC) for her technical support preparing the samples for RNA sequencing, Sarah van Leeuwen and Karen de Haan (Medical Microbiology, Amsterdam UMC) for their technical support in the culturing of the HBE cells and Nicole van der Wel (Electron Microscopy Center Amsterdam, Amsterdam UMC) for helping in the acquisition of electron microscopy images.

METHODS

Primary HBE cell culture

HBE cells were obtained anonymously from three patients undergoing a lobectomy for lung cancer at the Academic Medical Center, the Netherlands. Healthy tracheobronchial tissue was isolated distant from tumorous tissue by a pathologist and the absence of malignant cells was checked by microscopy. The Institutional Review Board of Amsterdam University Medical Center approved the study protocol (2015-122#A2301550) and written informed consent was obtained from the patients before sampling. Epithelial cells were isolated following the Fulcher's protocol.11 Briefly, passage 2 (P2) to P4 passaged HBE cells were expanded in human type IV placental collagen coated porous support 24-well Transwell inserts (Corning, Corning, NY, USA) for differentiation in PneumaCult-Ex Plus media (StemCell Technologies, Vancouver, Canada). When the cells were confluent in the inserts, the media was changed to PneumaCult-ALI medium (StemCell Technologies) containing penicillin and streptomycin on the basolateral side and the media on the apical side was removed, forming an air–liquid interface. The media were renewed every 2 or 3 days until full differentiation. Well-differentiated HBE cells were used on day 30 for stimulation in PneumaCult-ALI medium.

Cell stimulation

HBE cells were stimulated in PneumaCult-ALI medium with 1 µg/ ml flagellin from *Pseudomonas aeruginosa* (Invivogen, Toulouse, France), 100 ng/ml LPS from *Klebsiella pneumoniae* (L1519; Sigma, St. Louis, MO, USA), 1:2 (cell:bacteria) of UV-inactivated *Klebsiella pneumoniae* (ATCC 43816), *Pseudomonas aeruginosa* (ATCC 47085), or PBS added to the apical compartment. Unless stated otherwise, HBE cells were stimulated for 24 h. HBE cells were preincubated for 1 h prior to stimulation with vehicle, the glucose analog 2-DG (5 mM; Sigma) to inhibit glycolysis or the mTOR inhibitors rapamycin (10 nM; Cayman Chemical, Ann Arbor, MI, USA), BEZ235 (100 nM; BioVision, Milpitas, CA, USA) or torin-1 (100 nM; Tocris, Bristol, UK) added to the culture medium. After 1 h the bacterial stimuli (or PBS) were added to the apical side. Cell culture supernatants were stored at –80 °C until being analyzed. Cells were lysed in Lysis/Binding Buffer

(Roche, Basel, Switzerland) and stored at –80 °C for RNA isolation or directly stored at –80 °C until processed for western blot or metabolite measurements as described below.

Cytokine measurements

Human CXCL8, CCL20, CXCL1 and G-CSF, and mouse CXCL1 and CXCL2 were measured by ELISA according to manufacturer's instructions (R&D Systems, Minneapolis, MN, USA).

Reactive oxygen species and cell viability

For measurement of ROS, cells were stimulated for 24 h with vehicle (PBS) or flagellin and for the last 30 min, 10 µM of CarboxyH2DCFDA (Thermofisher, Waltham, MA, USA) was added. After stimulation, HBE cells were digested for 30 min at 37 °C with 5 mg/ ml Liberase TM (Sigma, St. Louis, MO, USA) and 10 mg/ml DNase (Roche). Data were acquired on a FACS Canto II cytometer (Becton Dickinson, Franklin Lakes, NJ, USA) and analyzed using FlowJo software (Treestaar Inc, Ashland, OR, USA). Fixable Viability Dye kit (eBioscience) was used to assess cell viability (>90% in all conditions).

Glucose and lactate measurements

Glucose and lactate were quantified using an enzymatic assay in which glucose and lactate were oxidized and the resulting H2O2 was coupled to the conversion of Amplex Red reagent to fluorescent resorufin by horseradish peroxidase (HRP) as described in ref. [18]

^{13}C-glucose labeling

For glucose labeling experiments, glucose-free RPMI media was supplemented with 2 mM [U-^{13}C]-glucose (Cambridge Isotope Laboratories, Tewksbury, MA, USA). Samples were separated in two phases as described previously[34]. Briefly, the aqueous phase was evaporated and the metabolite residue was processed on a SeQuant ZIC-cHILIC column (100 × 2.1 mm, 3 mm particle size, Merck, Darmstadt, Germany) coupled to a Bruker Impact II mass spectrometer (Bruker

Daltonic, Bremen, Germany). Data were analyzed using Bruker TASQ 2.0 software (Thermo Scientific, Waltham, MA, USA). ^{13}C enrichment was calculated based on mass distribution isotopomer analysis, results were corrected for their natural ^{13}C abundance by solving the associated set of linear equations for lactate using non-negative least squares[35].

Steady-state metabolomics

Metabolomics was performed as described previously[36]. For details see Supplementary Information.

mRNA extraction and RT-PCR

Total RNA was extracted from HBE cells using the High Pure RNA Isolation Kit (Roche) following the manufacturer's instructions. Reverse transcription was performed using the M-MLV Reverse Transcriptase (Promega, Madison, WI, USA) in the presence of RNase inhibitor (ThermoFisher) with 300 ng of DNase I (Roche) treated total RNA. RT-PCR was performed on LightCycler 480 (Roche) using the SensiFAST SYBR No-ROX Kit (Bioline, London, UK). Data are expressed as fold increases in expression, relative to the non-stimulated condition after normalization to HPRT as a housekeeping gene. Mitochondrial mass was determined as described in ref. [37] Briefly, gDNA was isolated using the AllPrep DNA/RNA mini kit (Qiagen, Hilden, Germany) and the ratio mtDNA/gDNA was calculated.

Total RNA was extracted from mouse epithelial brushes with Nucleospin RNA kits (Macherey-Nagel, Düren, Germany). RNA was reverse-transcribed with the High-Capacity cDNA Archive Kit (Applied Biosystems, Foster City, CA, USA). Gene expression was quantified by cDNA amplification in a QuantStudio 12 K real-time PCR system (Applied Biosystems), using Power SYBR® Green PCR Master Mix (Applied Biosystems). Relative mRNA levels were determined by comparing (1) the cycle thresholds (Ct) for the gene of interest and three calibrators *Actb*, *B2m*, and *Rpl13a* (ΔCt), and (2) the 2–ΔCt values for treated and control groups. The upper boundary for Ct was set to 35 cycles. Primers used in this study are listed in Table S1.

Immunoblot analysis

HBE cells were lysed in RIPA buffer supplemented with HALT protease and phosphatase inhibitor (ThermoFisher) and stored at –20 °C until processing. Samples were heat-denatured in reducing sample buffer (Laemmli buffer). Samples were loaded on either 10% or 4–20% polyacrylamide precast gels (Bio-Rad, Hercules, CA) and transferred to PVDF membranes. After incubation for 1 h with blocking buffer, immunoblotting was performed using antibodies to β-Actin (4967L; Cell Signaling, Danvers, MA), Erk (9107S; Cell Signaling), phospho S6 Ribosomal Protein (Ser235/236) (2211S; Cell Signaling), phospho-Akt (4060S; Cell Signaling), or phospho4EBP1 (9459S; Cell Signaling). Goat anti-rabbit (7074S; Cell Signaling) and goat anti-mouse (7076S; Cell Signaling) HRP antibodies were used as secondary antibodies. Blots were incubated with the Lumi-Light detection kit (Roche) and pictures were taken using ImageQuant LAS-4000 (GE Healthcare, Chicago, IL, USA).

RNA library preparation and sequencing

RNA was isolated from HBE cells (from three distinct donors in duplicates for each condition) as described above. RNA quality was assessed by bioanalysis (Agilent, Santa Clara, CA), with all samples having RNA integrity numbers >7. Total RNA concentrations were determined by Qubit® 2.0 Fluorometer (Life Technologies, Carlsbad, CA, USA). Sequencing libraries were prepared by means of the KAPA RNA HyperPrep with RiboErase (Roche) as per manufacturer's instructions. Libraries were sequenced using the Illumina HiSeq4000 (Illumina, San Diego, CA, USA) to generate 50 bp single-end reads.

Bioinformatics analysis of RNAseq

The sequence read quality was assessed using FastQC methods (version 0.11.5; Babraham Institute, Babraham, Cambridgeshire, UK). Trimmomatic version 0.3238 was used to trim the Illumina adapters and filter low quality reads and ambiguous nucleotide-containing sequences. Low quality leading (three nucleotides) and trailing (three nucleotides) bases were removed from each read. A sliding window trimming using a window of four and a phred score threshold of

15 nucleotides was used to access the quality of the reads. After preprocessing, the remaining high-quality reads were aligned against the Genome Reference Consortium Human Genome Build 38 patch release 7 (GRCh38.p7) using Bowtie2 version 2.3.4.339 with default parameters. Count data were generated by means of the FeatureCounts method[40], and differential expression analyzed using the DESeq2 method[41] in the R statistical computing environment (R Core Team 2014. R: A language and environment for statistical computing. R Foundation for Statistical Computing, Vienna, Austria). Throughout significance was calculated using Benjamini–Hochberg adjusted p values[42]. Using the Reactome pathway knowledgebase[43], the GSEA approach[19] was applied to determine, for any given pathway, whether a predefined set of genes (Reactome pathways) showed statistically significant differences between two conditions.

Electron microscopy

To assess mitochondrial morphology HBE cells were fixed in Mc Dowell containing paraformaldehyde and glutaraldehyde (Polyzciences, Inc., Warrington, PA) embedded in gelatin and small blocks of gelatin embedded cells were postfixed with 1% osmium tetroxide (OsO4, Electron microscopy sciences, Hatfield, PA; in cacodylate buffer). Subsequently, the samples were dehydrated in an alcohol series and embedded into Epon (LX-112 resin Ladd research, Wiliston, VT) and 70 nm thin sections were made with an ultramicrotome (Leica UC6). Sections were analyzed with a FEI Tecnai-12 G2 Spirit Biotwin electron microscope (Fei/ThermoFisher, Eindhoven, The Netherlands), and images were made with a Veleta camera using Radius Software (EMSIS, Münster, Germany).

Mice

Six- to eight-week-old female C57BL/6JRj mice (Janvier Labs, Saint-Berthevin, France) were housed in a pathogen-free facility in compliance with institutional guidelines (#C59-350009, Institut Pasteur de Lille). All experimental procedures were approved by the local animal care and use committee and by the French Ministry of Research (authorization APAFIS#5165— 2015121722376405_v2). Mice were administered with rapamycin intraperitoneally (4 mg/kg; Cayman Chemical) or vehicle (2% DMSO in PBS) 24 and 1 h prior to intranasal

administration of 0.5 µg ultrapure flagellin from P. aeruginosa (Invivogen). After 2 h, BAL fluid samples were obtained as described before[17]. Briefly, the trachea was cannulated via a midline incision and 2 × 0.3 ml of sterile PBS was instilled to retrieve the BAL fluid. Thereafter, bronchial brushes were performed as described by Chen *et al.*[44] and qPCR analyses were performed as described above. In short, sanded PE50 tubing (P240 sandpaper) treated with RNaseZap were inserted into the main bronchus via the trachea with gentle brushing and immediately processed for RNA extraction.

Quantification and statistical analysis

All the analyses were done using GraphPad Prism 7.03. The number of replicates and the statistical tests used for each data set are described in the figure legends. In most cases, Student's *t* test was used. A p value < 0.05 was considered statistically significant.

REFERENCES

1. Hiemstra, P. S., McCray, P. B. & Bals, R. The innate immune function of airway epithelial cells in inflammatory lung disease. Eur. Respir. J. 45, 1150–1162 (2015).
2. Whitsett, J. A. & Alenghat, T. Respiratory epithelial cells orchestrate pulmonary innate immunity. Nat. Immunol. 16, 27–35 (2015).
3. Hasan, S., Sebo, P. & Osicka, R. A guide to polarized airway epithelial models for studies of host-pathogen interactions. FEBS J. 285, 4343–4358 (2018).
4. Stienstra, R., Netea-Maier, R. T., Riksen, N. P., Joosten, L. A. B. & Netea, M. G. Specific and complex reprogramming of cellular metabolism in myeloid cells during innate immune responses. Cell Metab. 26, 142–156 (2017).
5. Jung, J., Zeng, H. & Horng, T. Metabolism as a guiding force for immunity. Nat. Cell Biol. 21, 85–93 (2019).
6. O'Neill, L. A. J., Kishton, R. J. & Rathmell, J. A guide to immunometabolism for immunologists. Nat. Rev. Immunol. 16, 553–565 (2016).
7. Weichhart, T., Hengstschläger, M. & Linke, M. Regulation of innate immune cell function by mTOR. Nat. Rev. Immunol. 15, 599–614 (2015).
8. Eisenreich, W., Rudel, T., Heesemann, J. & Goebel, W. How viral and intracellular bacterial pathogens reprogram the metabolism of host cells to allow their intracellular replication. Front. Cell Infect. Microbiol. 9, 42 (2019)
9. Dechecchi, M. C. et al. Modulators of sphingolipid metabolism reduce lung inflammation. Am. J. Respir. Cell Mol. Biol. 45, 825–833 (2011).
10. McClendon, J. et al. Hypoxia-inducible factor 1α signaling promotes repair of the alveolar epithelium after acute lung injury. Am. J. Pathol. 187, 1772–1786 (2017).
11. Fulcher, M. L. & Randell, S. H. Human nasal and tracheo-bronchial respiratory epithelial cell culture. Methods Mol. Biol. 945, 109–121 (2013).
12. Karelehto, E. et al. Polarized entry of human parechoviruses in the airway epithelium. Front. Cell Infect. Microbiol. 8, 294 (2018).
13. McIsaac, S. M., Stadnyk, A. W. & Lin, T.-J. Toll-like receptors in the host defense against *Pseudomonas aeruginosa* respiratory infection and cystic fibrosis. J. Leukoc. Biol. 92, 977–985 (2012).
14. Vijayan, A., Rumbo, M., Carnoy, C. & Sirard, J.-C. Compartmentalized antimicrobial defenses in response to flagellin. Trends Microbiol. 26, 423–435 (2018).
15. Golebski, K. et al. Fc γ RIII stimulation breaks the tolerance of human nasal epithelial cells to bacteria through cross-talk with TLR4. Mucosal Immunol. 12, 425–433 (2019).
16. Van Maele, L. et al. Airway structural cells regulate TLR5-mediated mucosal adjuvant activity. Mucosal Immunol. 7, 489–500 (2014).

17. Anas, A. A. et al. Lung epithelial MyD88 drives early pulmonary clearance of *Pseudomonas aeruginosa* by a flagellin dependent mechanism. Am. J. Physiol. Lung Cell Mol. Physiol. 311, L219–L228 (2016).
18. Lachmandas, E. et al. Microbial stimulation of different Toll-like receptor signaling pathways induces diverse metabolic programmes in human monocytes. Nat. Microbiol. 2, 1–10 (2016).
19. Yu, G. & He, Q. Y. ReactomePA: an R/Bioconductor package for reactome pathway analysis and visualization. Mol. Biosyst. 12, 477–479 (2016).
20. Cheng, S.-C. et al. Broad defects in the energy metabolism of leukocytes underlie immunoparalysis in sepsis. Nat. Immunol. 17, 406–413 (2016).
21. Lachmandas, E. et al. Rewiring cellular metabolism via the AKT/mTOR pathway contributes to host defence against Mycobacterium tuberculosis in human and murine cells. Eur. J. Immunol. 46, 2574–2586 (2016).
22. Smallwood, H. S. et al. Targeting metabolic reprogramming by influenza infection for therapeutic intervention. Cell Rep. 19, 1640–1653 (2017).
23. Buck, M. D., O'Sullivan, D. & Pearce, E. L. T cell metabolism drives immunity. J. Exp. Med. 212, 1345–1360 (2015).
24. Keating, R. & McGargill, M. A. mTOR regulation of lymphoid cells in immunity to pathogens. Front. Immunol. 7, 180 (2016).
25. Brognard, J., Sierecki, E., Gao, T. & Newton, A. C. PHLPP and a second isoform, PHLPP2, differentially attenuate the amplitude of Akt signaling by regulating distinct Akt isoforms. Mol. Cell 25, 917–931 (2007).
26. Weichhart, T. et al. The TSC-mTOR signaling pathway regulates the innate inflammatory response. Immunity 29, 565–577 (2008).
27. Lorne, E. et al. Participation of mammalian target of rapamycin complex 1 in Tolllike receptor 2- and 4-induced neutrophil activation and acute lung injury. Am. J. Respir. Cell Mol. Biol. 41, 237–245 (2009).
28. Hu, Y. et al. Activation of MTOR in pulmonary epithelium promotes LPS-induced acute lung injury. Autophagy 12, 2286–2299 (2016).
29. Bao, W. et al. mTORC1 regulates flagellin-induced inflammatory response in macrophages. PLoS ONE 10, e0125910 (2015).
30. Rimessi, A. et al. Mitochondrial Ca2+-dependent NLRP3 activation exacerbates the Pseudomonas aeruginosa-driven inflammatory response in cystic fibrosis. Nat. Commun. 6, 6201 (2015).
31. Jia, X., Cao, B., An, Y., Zhang, X. & Wang, C. Rapamycin ameliorates lipopolysaccharide-induced acute lung injury by inhibiting IL-1β and IL-18 production. Int. Immunopharmacol. 67, 211–219 (2019).

32. Zhang, Z., Louboutin, J.-P., Weiner, D. J., Goldberg, J. B. & Wilson, J. M. Human airway epithelial cells sense Pseudomonas aeruginosa infection via recognition of flagellin by Toll-like receptor 5. Infect. Immun. 73, 7151–7160 (2005).
33. Wang, R. et al. Airway epithelial expression of TLR5 is downregulated in healthy smokers and smokers with chronic obstructive pulmonary disease. J. Immunol. 189, 2217–2225 (2012).
34. Held, N. M. et al. Pyruvate dehydrogenase complex plays a central role in brown adipocyte energy expenditure and fuel utilization during short-term beta-adrenergic activation. Sci. Rep. 8, 9562 (2018).
35. Fernandez-Fernandez, M. & Rodriguez-Gonzalez, P. Garcia & Alonso, J. I. A simplified calculation procedure for mass isotopomer distribution analysis (MIDA) based on multiple linear regression. J. Mass Spectrom. 51, 980–987 (2016).
36. Molenaars, M. et al. A conserved mito-cytosolic translational balance links two longevity pathways. Cell Metab. 31, 549–563.e7 (2020).
37. Rooney, J. P. et al. PCR based determination of mitochondrial DNA copy number in multiple species. Methods Mol. Biol. 1241, 23–38 (2015).
38. Bolger, A. M., Lohse, M. & Usadel, B. Trimmomatic: a flexible trimmer for Illumina sequence data. Bioinformatics 30, 2114–2120 (2014).
39. Langmead, B. & Salzberg, S. L. Fast gapped-read alignment with Bowtie 2. Nat. Methods 9, 357–359 (2012).
40. Liao, Y., Smyth, G. K. & Shi, W. FeatureCounts: an efficient general purpose program for assigning sequence reads to genomic features. Bioinformatics 30, 923– 930 (2014).
41. Love, M. I., Huber, W. & Anders, S. Moderated estimation of fold change and dispersion for RNA-seq data with DESeq2. Genome Biol. 15, 550 (2014).
42. Benjamini, Y. & Hochberg, Y. Controlling the false discovery rate: a practical and powerful approach to multiple testing. J. R. Stat. Soc. Ser. B. 57, 289–300 (1995).
43. Fabregat, A. et al. The reactome pathway knowledgebase. Nucleic Acids Res. 311, L219–L228 (2016). 44. Chen, K. et al. IL-17 receptor signaling in the lung epithelium is required for mucosal chemokine gradients and pulmonary host defense against K. pneumoniae. Cell Host Microbe. 20, 596–605 (2016).

SUPPLEMENTARY MATERIAL

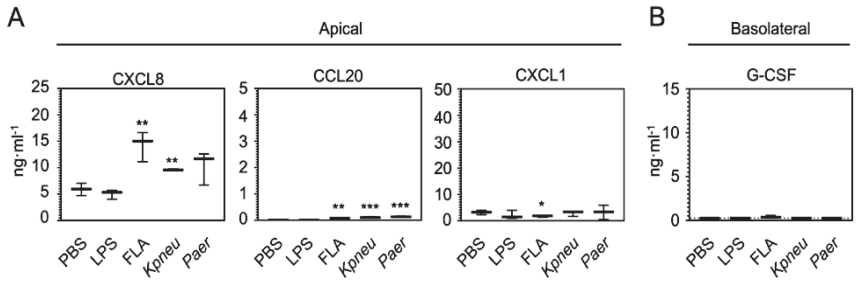

Figure S1. Polarized release of chemokines and transcriptomic changes induced by flagellin in HBE cells

(**A** and **B**) CXCL8, CCL20 and CXCL1 levels in the apical wash (**A**) and G-CSF levels in the basolateral compartment (**B**) of HBE cells untreated (PBS) or stimulated for 24 hours with LPS (100 ng/ml), flagellin (1 μg/ml), UV-inactivated *Klebsiella pneumoniae* or *Pseudomonas aeruginosa*. Data are presented in box and whisker plots (n = 3 - 4 per group). P values were calculated using Student's *t* test compared to unstimulated cells. *p < 0.05; **p < 0.01; ***p < 0.001.

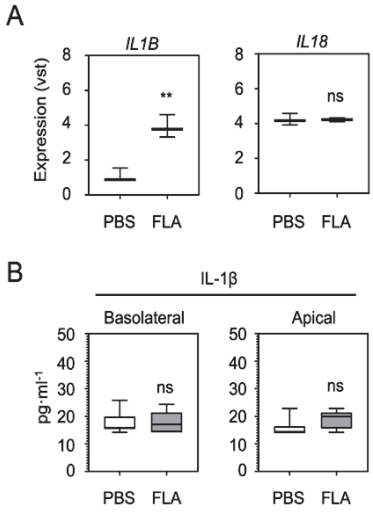

Figure S2. Effect of flagellin on *IL1B* and *IL18* gene expression and IL-1β release

(**A**) Expression of *IL1B* and *IL18* genes in flagellin or PBS stimulated HBE cells (24-hour incubation). Data are presented in box and whisker plots (n = 6 from 3 biological donors in duplicate from 2 independent experiments). P values were calculated using Student's paired *t* test. **p < 0.01. ns, not significant. vst, variance stabilizing transformed (expression).

(**B**) IL-1β levels in culture supernatant and apical washes of HBE cells incubated with flagellin or PBS. Data are presented in box and whisker plots (n = 5 - 7 replicates pooled from two independent experiments). P values were calculated using Student's paired *t* test. ns, not significant.

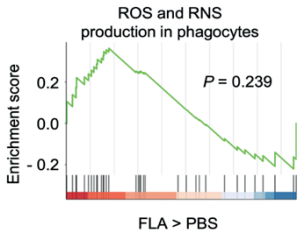

Figure S3. ROS production pathway analysis

Enrichment plot of the ROS production pathway in HBE cells activated with flagellin for 24 hours compared to unstimulated control cells (PBS), identified by GSEA. Data from 3 biological individuals in duplicate from 2 independent experiments (n = 6).

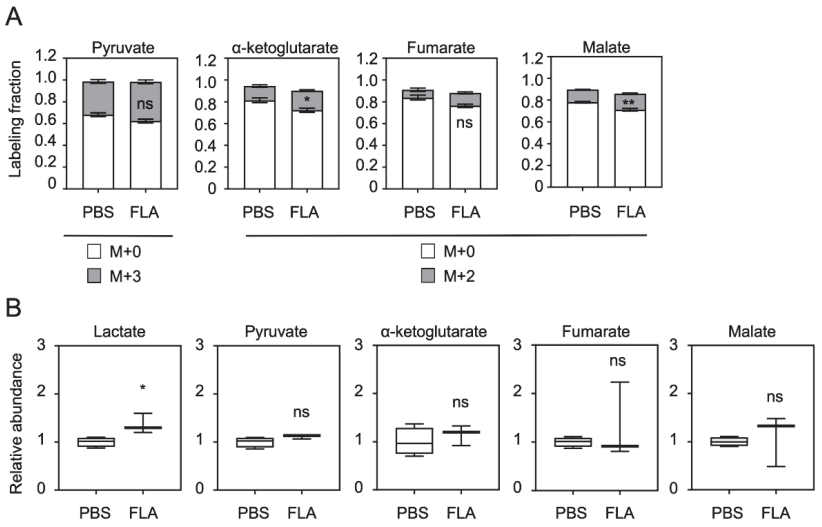

Figure S4. Flux-omics and steady-state metabolomics

(*A*) Glucose-derived carbon labeling of pyruvate, α-ketoglutarate, fumarate and malate in HBE cells 30 minutes after incubation with flagellin or PBS (control) in ^{13}C-glucose-containing media. Bar graphs show mass isotopologue distribution of incorporated label. M+0 bars represent the fraction of metabolite with no ^{13}C-glucose incorporation.

(*B*) Relative abundance of glycolysis and TCA-metabolites measured by liquid chromatography-high resolution mass spectrometry (LC-HRMS).

Data in (*A*) comprises 3 replicates per condition and 3 or 4 replicates in (*B*).

P values were calculated using Student's *t* test. *$p < 0.05$; **$p < 0.01$; ns, not significant.

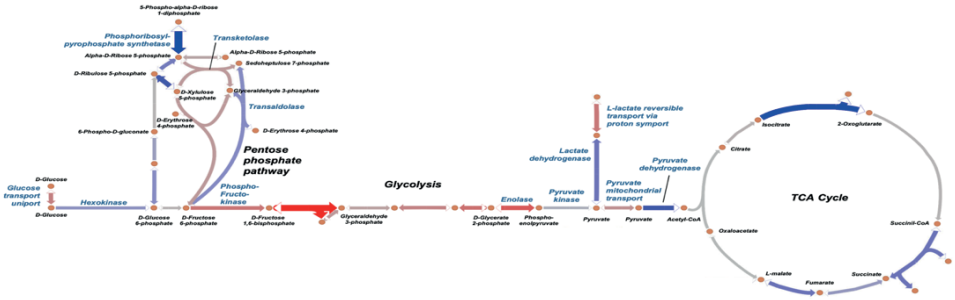

Figure S5. Schematic pathway representation of carbohydrate metabolism genes
Schematic representation of gene expression in the main metabolism pathways in HBE cells after 24 hours stimulation with flagellin. Each arrow represents an enzymatic reaction catalyzed by an enzyme (encoded by known genes) between two metabolites depicted by dots. Red denotes over-expression and blue under-expression of the gene involved in the reaction. A darker color indicates a bigger change in transcript levels. The data shown illustrate that genes involved in glycolysis are upregulated in response to flagellin, whereas genes involved in the pentose phosphate pathway and TCA cycle are downregulated. Data from 3 biological individuals in duplicate from 2 independent experiments (n = 6).

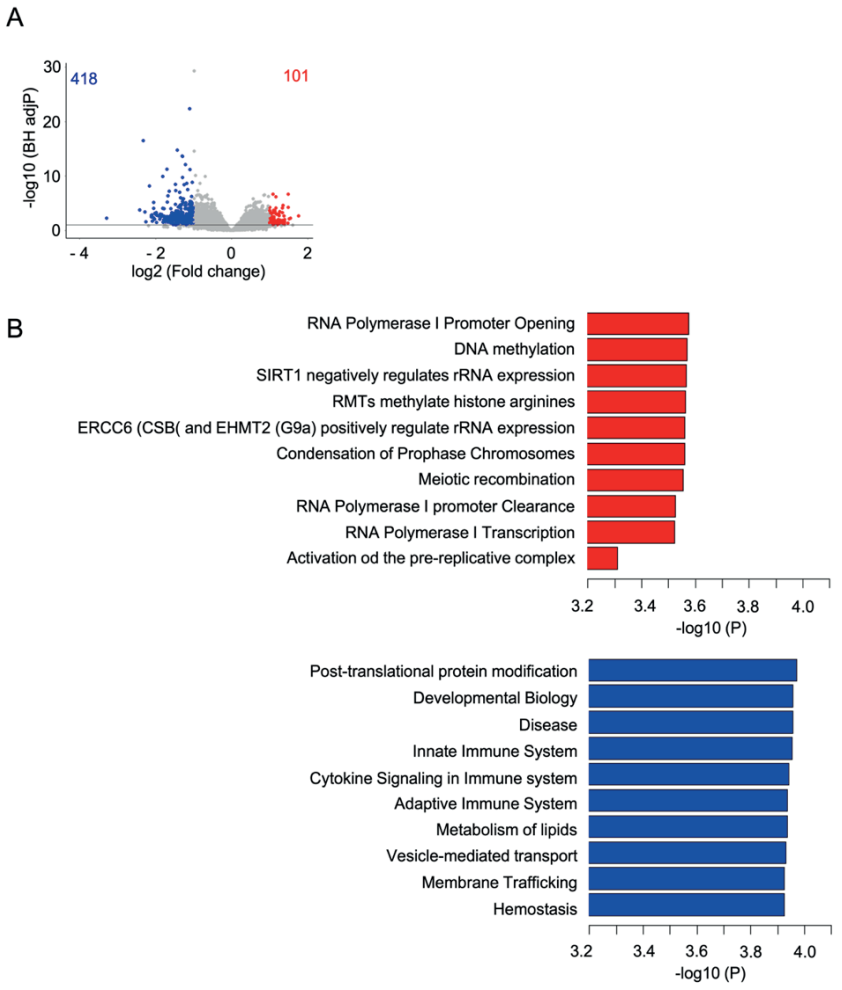

Figure S6. Genome-wide transcriptome RNAseq analysis of flagellin stimulated HBE cells in the presence of rapamycin

(**A**) Volcano plot presentation (integrating multiple-test adjusted p-values and log2 fold changes) of genome-wide transcriptome analysis of HBE cells stimulated with flagellin for 24 hours. Numbers in red and blue indicate number of genes with significantly upregulated or downregulated gene expression, respectively in the presence of rapamycin (10 nM) relative to that in the presence of vehicle. Horizontal line represents the multiple-test adjusted significance threshold (Benjamini-Hochberg adjusted $p < 0.05$).

(**B**) Pathway analysis from (**A**) showing pathways enriched for up-regulated (red) or down-regulated genes (blue).

Data from 3 biological individuals in duplicate from 2 independent experiments (n = 6).

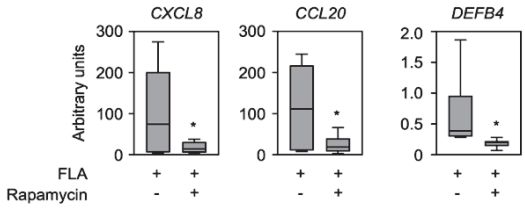

Figure S7. RT-PCR validation of RNAseq data

mRNA expression for the indicated immune mediators (normalized to the house-keeping gene *HPRT*) in HBE cells pre-incubated for 1 hour with 10 nM rapamycin or vehicle after 24 hours stimulation with flagellin. Data are presented as box and whisker plots (n = 6 from 3 biological individuals in duplicate from 2 independent experiments). P values were calculated using Student's *t* test. *$p < 0.05$.

Gene	Primer	Sequence 5'-3'
h*HPRT*	HPRT-Fwd	GGATTTGAAATTCCAGACAAGTTT
	HPRT-Rev	GCGATGTCAATAGGACTCCAG
h*DEFB4A*	DEFB4A-Fwd	CTCCTCTTCTCGTTCCTCTTCA
	DEFB4A-Rev	GCAGGTAACAGGATCGCCTAT
h*CCL20*	CCL20-Fwd	TGCTGTACCAAGAGTTTGCTC
	CCL20-Rev	CGCACACAGACAACTTTTTCTTT
h*CXCL8*	CXCL8-Fwd	AACCTTTCCACCCCAAATTTAT
	CXCL8-Rev	AAAACTTCTCCACAACCCTCTG
h*CXCL1*	CXCL1-Fwd	GCATACTGCCTTGTTTAATGGT
	CXCL1-Rev	CCAGTAAAGGTAGCCCTTGTTTC
h*CSF3*	CSF3-Fwd	AAGGGATCTCCCCCGAGTTG
	CSF3-Rev	CAGATGGTGGTGGCAAAGTC
h*MT-TL1*	MT-TL1-Fwd	CACCCAAGAACAGGGTTTGT
	MT-TL1-Rev	TGGCCATGGGTATGTTGTTA
h*B2M*	B2M-Fwd	TGCTGTCTCCATGTTTGATGTATCT
	B2M-Rev	TCTCTGCTCCCCACCTCTAAGT
m*Actb*	Actb-Fwd	CTCTGGCTCCTAGCACCATGAAGA
	Actb-Rev	GTAAAACGCAGCTCAGTAACAGTCCG
m*Hk2*	Hk2-Fwd	GTGTGCTCCGAGTAAGGGTG
	Hk2-Rev	CAGGCATTCGGCAATGTGG
m*Cxcl1*	Cxcl1-Fwd	CTTGGTTCAGAAAATTGTCCAAAA
	Cxcl1-Rev	CAGGTGCCATCAGAGCAGTCT

m*Cxcl2*	Cxcl2-Fwd	CCCTCAACGGAAGAACCAAA
	Cxcl2-Rev	CACATCAGGTACGATCCAGGC
m*Csf3*	Csf3-Fwd	CCTGGAGCAAGTGAGGAAGA
	Csf3-Rev	CAGCTTGTAGGTGGCACACA

Table S.1. Primers used for qPCR

SUPPLEMENTARY METHODS

Steady-state metabolomics

One part of chloroform was added to one part of methanol/water (1/1) to the dry cell-pellet and centrifugated for 10 min at 14000 rpm. The polar phase was then dried using a vacuum concentrator at 60°C and reconstituted in 100 μL methanol/water (6/4; v/v). Metabolites were analyzed using a Thermo Scientific ultra-high pressure liquid chromatography system (Waltman, MA, USA) coupled to Thermo Q Exactive (Plus) Orbitrap mass spectrometer (Waltman). Chromatographic separation was performed using a Merck Millipore SeQuant ZIC-cHILIC column (PEEK 100 x 2.1 mm, 3 μm particle size). Mobile phase consisted of (1) 1:9 acetonitrile:water and (2) 9:1 acetonitrile:water, both containing 5 mM ammonium acetate. Using a flow rate of 0.25 mL/min, the LC gradient consisted of: 100% B for 0-2 min, ramp to 0% B at 28 min, 0% B for 28-30 min, ramp to 100% B at 31 min, 100% B for 31-35 min. MS data were acquired using negative and positive ionization in full scan mode over the range of m/z 50-1200. Data were analyzed using Xcalibur software (version 3.0, Thermo scientific). Metabolites abundance were normalized to internal standards. For metabolite identification, a combination of accurate mass, (relative) retention times and fragmentation spectra, compared to the analysis of a library of standards were used.